Hindawi
Journal of Applied Mathematics
Volume 2019, Article ID 3472518, 16 pages
https://doi.org/10.1155/2019/3472518

Research Article

Finite Element Method Solution of Boundary Layer Flow of Powell-Eyring Nanofluid over a Nonlinear Stretching Surface

Wubshet Ibrahim [1] **and Gosa Gadisa** [2]

[1] *Department of Mathematics, Ambo University, Ambo, Ethiopia*
[2] *Department of Mathematics, Wollega University, Nekemte, Ethiopia*

Correspondence should be addressed to Wubshet Ibrahim; wubshetib@yahoo.com

Received 13 February 2019; Revised 10 May 2019; Accepted 28 May 2019; Published 4 July 2019

Academic Editor: Dogan Kaya

The nonlinear convective flow of Eyring-Powell nanofluid using Catteneo-Christov model with heat generation or absorption term and chemical reaction rate over nonlinear stretching surface is analyzed. The simultaneous nonlinear partial differential equations governing the boundary layer flow are transformed to the corresponding nonlinear ordinary differential equations using similarity solution and then solved using Galerkin finite element method (GFEM). The impacts of pertinent governing parameters like Brownian diffusion, thermophoresis, mixed convection, heat generation or absorption, chemical reaction rate, Deborah numbers, Prandtl number, magnetic field parameter, Lewis number, nonlinear stretching sheet, and Eyring-Powell fluid parameters on velocity field, temperature, and nanoparticle concentration are given in both figures and tabular form. The result shows that the rise in chemical reaction rate will improve mass transfer rate and reduce heat transfer rate and local buoyancy parameter has quit opposite effect. The attributes of local skin friction coefficient, Nusselt number, and Sheer wood number are investigated and validated with existing literatures.

1. Introduction

Due to wide application of non-Newtonian fluids in the advancement of modern technologies, many researchers engaged to explore the non-Newtonian fluid. The investigators exposed that non-Newtonian fluids are applicable in polymer devolatilization and processing, heat exchangers, extrusion process, wire and fiber coating, chemical processing equipment, etc. Different researchers studied different non-Newtonian models by different solution method. Modeling of the viscoelastic properties of polymers has often been a very hot subject. The viscoelastic constitutive equations have been developed for the understanding of the numerous means of deformation and flow but unluckily have not offered us quantitative prophetic power. Extremely often the predictions depend on the model applied for the computations and are not confirmed with experimental observations. Few viscoelastic boundary layer flow problems can be solved with the suitable constitutive equations, but this is still an area of academic research with partial practical applications at the moment.

Most of the products we enjoy today in our daily life are invented from polymers. Some of them are house wares, toys, knobs, appliance parts, electrical fixtures, toothbrushes, cups, handles, lids, and packages. The Eyring-Power law model which is often used in chemical engineering is also capable of modelling these complex fluid flows under general flow conditions. Many fluids do not exhibit the same type of rheological attributes. They exhibit Newtonian character for a range of shear stresses and non-Newtonian character for some other ranges of shear stresses. In some cases, these types of fluids are suitable to be investigated. Among this kind of scenario, the present study paid attention to Eyring-Powell model which has more advantage as a result of its reduction to Newtonian model for smaller and larger shear rates. To give clear insight on non-Newtonian flow especially Eyring-Powell fluid, recently much research has been conducted. We discuss few of them as follows.

Satyaban *et al.* [1] studied mixed convective flow of a Powell-Eyring fluid over a nonlinear stretching surface with thermal diffusion and diffusion thermo. Khan et *al.* [2] analyzed flow of an Eyring-Powell fluid over a stretching sheet. Gaffar *et al.* [3] investigated non-Newtonian thermal convection of Eyring-Powell fluid from an isothermal sphere with Biot number effects. Obaid *et al.* [4] studied entropy generation in MHD Eyring–Powell fluid flow over an unsteady oscillatory porous stretching surface under the impact of thermal radiation and heat source/sink. The effect of Cattaneo-Christov heat flux model for Eyring-Powell fluid over an exponentially stretching sheet is discussed by Ahmad and Iqbal [5]. The boundary layer flow of the non-Newtonian power-law fluid past the nonlinear stretching sheet has been analyzed by Megahed [6, 7]. Later on, Megahed [8] introduced the concepts of flow and heat transfer of non-Newtonian Sisko fluid past a nonlinearly stretching sheet with heat generation and viscous dissipation. Upadhay and Raju [9] explored Cattaneo-Christov on heat and mass transfer of unsteady Eyring-Powell dusty nanofluid over sheet with heat and mass flux conditions. Kumar *et al.* [10] discussed the concept of magnetohydrodynamic Cattaneo-Christov flow past a cone and a wedge with variable heat source/sink. Later on, Kumar *et al.* [11] introduced impact of nonlinear radiation on MHD nonaligned stagnation point flow of micropolar fluid over a convective surface. Beside this, Kumar *et al.* [12] investigated the impact of Brownian motion and thermophoresis on bioconvective flow of nanoliquids past a variable thickness surface with slip effects.

Hayat *et al.* [13] described MHD nonlinear stretching flow of Powell–Eyring nanomaterial. Madhu and Kishan [14] derived MHD boundary-layer flow of a non-Newtonian nanofluid past a stretching sheet with a heat source/sink. Rahimi *et al.* [15] presented solution of the boundary layer flow of an Eyring-Powell non-Newtonian fluid over a linear stretching sheet by collocation method. Akinshilo and Olaye [16] explained the analysis of the Eyring-Powell model based fluid flow in a pipe with temperature dependent viscosity and internal heat generation. Madhu and Kishan [17] analyzed finite element analysis of heat and mass transfer by MHD mixed convection stagnation-point flow of a non-Newtonian power-law nanofluid towards a stretching surface with radiation. Babu *et al.* [18] described free convective MHD Cattaneo-Christov flow over three different geometries with thermophoresis and Brownian motion.

Moreover, large temperature difference between the surface and the ambient fluid forces the researchers to investigate the nonlinear density temperature (NDT) difference in the buoyancy force term due to its major influence on the flow and heat transfer characteristics. Vajravelu and Sastri [19] investigated the flow between two parallel plates in view of the quadratic density temperature (QDT) variation and reported that the flow and heat transfer rates are considerably affected by it. The fully developed free convection flow in circular pipe with nonlinear density temperature variations was studied by Bhargava and Agarwal [20]. Khan *et al.* [21] investigated entropy generation in radiative motion of tangent hyperbolic nanofluid in presence of activation energy and nonlinear mixed convection. The nonlinear convection effects on the flow past a flat porous plate have been investigated by Vajravelu et al. [22]. Khan *et al.* [23] studied the numerical simulation of nonlinear thermal radiation and homogeneous-heterogeneous reactions in convective flow by a variable thickened surface.

Most recently, Hayat and Nadeem [24] solved flow of 3D Eyring-Powell fluid by utilizing Cattaneo-Christov heat flux model and chemical processes over an exponentially stretching surface. In the same year, Saima and Noreen [25] presented magneto-thermo-hydrodynamic peristaltic flow of Eyring-Powell nanofluid in asymmetric channel. Later on, Wubshet Ibrahim and Bullo Hindebu [26] analyzed MHD boundary layer flow of Eyring-Powell nanofluid past stretching cylinder with Cattaneo-Christov heat flux model. Kumar *et al.* [27] analyzed impact of Lorentz force on unsteady bioconvective flow of Carreau fluid across a variable thickness sheet with non-Fourier heat flux model. Ramadevi *et al.* [28] scrutinized MHD flow of Carreau fluid over a variable thickness melting surface subject to Cattaneo-Christov heat flux. Kumar *et al.* [29] have been studying MHD Carreau fluid flow past a melting surface with Cattaneo-Christov heat flux.

From the surveyed literatures above, it has been observed that the problem of nonlinear convective flow of magneto-hydrodynamic (MHD) boundary layer flow of an Eyring-Powell nanofluid using Catteneo-Christov model with heat generation/absorption and chemical reaction term past nonlinear stretching surface is still limited. Additional effects of local buoyancy parameter, local heat generation, chemical reaction rate, nonlinear stretching sheet parameter, and the technique used to solve the problem are added features to the uniqueness.

Thus, the main target of the present study is to analyze nonlinear convective flow of two-dimensional steady laminar incompressible magnetohydrodynamic (MHD) boundary layer flow of an electrically conducting Eyring-Powell nanofluid using Catteneo-Christov model with heat generation/absorption and chemical reaction over nonlinear stretching surface. The impacts of diverse governing variables on fluid velocity, temperature of the fluid, and nanoparticle concentration profile of laminar boundary layer flow are presented in both graphs and tabular form. The numerical method employed to solve the current problem is Galerkin finite element method (GFEM) [21–30].

2. Mathematical Formulation of the Problem

We analyze a nonlinear convective flow of two-dimensional steady laminar incompressible magnetohydrodynamic (MHD) boundary layer flow of Eyring-Powell nanofluid using Catteneo-Christov model with heat generation or absorption and chemical reaction over nonlinear stretching surface. The diagram of the targeted incompressible boundary layer flow is illustrated in Figure 1. The x-axis is considered along the nonlinear stretching surface and the y-axis is taken normal to it. The surface is extended with a nonlinear velocity $u_w(x) = ax^n$, where $a > 0$ is constant. The induced magnetic field is ignored owing to small Reynolds number.

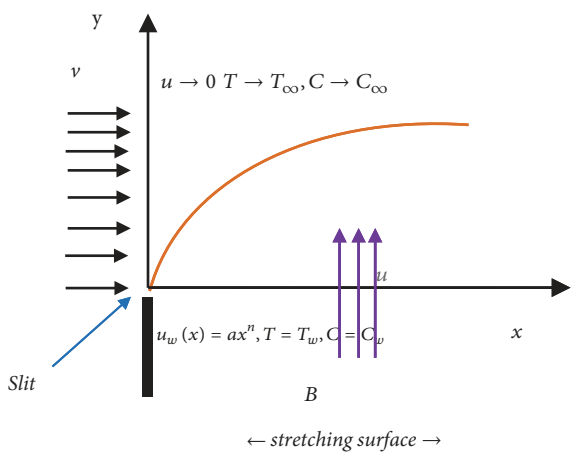

Figure 1: Geometry of the problem.

The extra stress tensor for Powell-Eyring fluid is given by [30]

$$\tau_{ij} = \mu \frac{\partial u_i}{\partial x_j} + \frac{1}{\beta^*} \sinh^{-1}\left(\frac{1}{c^*}\frac{\partial u_i}{\partial x_j}\right), \tag{1}$$

where μ represents dynamic viscosity and β^* and c^* stand for materials constants.

Assuming

$$\sinh^{-1}\left(\frac{1}{c^*}\frac{\partial u_i}{\partial x_j}\right) \cong \frac{1}{c^*}\frac{\partial u_i}{\partial x_j} - \frac{1}{6}\left(\frac{1}{c^*}\frac{\partial u_i}{\partial x_j}\right)^3, \quad \left|\frac{1}{c^*}\frac{\partial u_i}{\partial x_j}\right| << 1, \tag{2}$$

the governing equations for the boundary layer flow are

$$\frac{\partial u}{\partial x} + \frac{\partial v}{\partial y} = 0 \tag{3}$$

$$u\frac{\partial u}{\partial x} + v\frac{\partial u}{\partial y} = \left(\nu + \frac{1}{\rho_f \beta^* c^*}\right) - \frac{1}{2\rho\beta^* c^{*^3}}\left(\frac{\partial u}{\partial y}\right)^2 \frac{\partial^2 u}{\partial y^2} - \frac{\sigma B_0^2}{\rho_f} u + g\Lambda_1 (T - T_\infty) + g\Lambda_2 (T - T_\infty)^2 + g\Lambda_3 (C - C_\infty) + g\Lambda_4 (C - C_\infty)^2 \tag{4}$$

$$u\frac{\partial T}{\partial x} + v\frac{\partial T}{\partial y} + \lambda_E\left(u\frac{\partial u}{\partial x}\frac{\partial T}{\partial x} + v\frac{\partial v}{\partial y}\frac{\partial T}{\partial y} + u\frac{\partial v}{\partial x}\frac{\partial T}{\partial y} + v\frac{\partial u}{\partial y}\frac{\partial T}{\partial x} + 2uv\frac{\partial^2 T}{\partial x \partial y} + u^2\frac{\partial^2 T}{\partial x^2} + v^2\frac{\partial^2 T}{\partial y^2}\right) = \alpha_f \frac{\partial^2 T}{\partial y^2} + \tau\left\{D_B\left(\frac{\partial T}{\partial y}\frac{\partial C}{\partial y}\right) + \frac{D_T}{T_\infty}\left(\frac{\partial T}{\partial y}\right)^2\right\} + \frac{Q}{\rho_f c_p}(T - T_\infty) \tag{5}$$

$$u\frac{\partial C}{\partial x} + v\frac{\partial C}{\partial y} + \lambda_C\left(u\frac{\partial u}{\partial x}\frac{\partial C}{\partial x} + v\frac{\partial v}{\partial y}\frac{\partial C}{\partial y} + u\frac{\partial v}{\partial x}\frac{\partial C}{\partial y} + v\frac{\partial u}{\partial y}\frac{\partial C}{\partial x} + 2uv\frac{\partial^2 C}{\partial x \partial y} + u^2\frac{\partial^2 C}{\partial x^2} + v^2\frac{\partial^2 C}{\partial y^2}\right) = D_B\frac{\partial^2 C}{\partial y^2} + \frac{D_T}{T_\infty}\frac{\partial^2 T}{\partial y^2} - k_1 (C - C_\infty) \tag{6}$$

with appropriate boundary condition

$$\begin{aligned} &u = u_w(x) = ax^n, \\ &v = 0 \qquad \text{at } y = 0 \\ &u \longrightarrow 0 \quad \text{as } y \longrightarrow \infty \\ &T = T_w, \\ &C = C_w \qquad \text{at } y = 0 \\ &T \longrightarrow T_\infty, \\ &C \longrightarrow C_\infty \qquad \text{as } y \longrightarrow \infty, \end{aligned} \tag{7}$$

where u and v are the velocity components in the x and y directions, ν is the kinematic viscosity, u_w is the stretching velocity, g is the gravitational acceleration, Λ_1 and Λ_2 are linear and nonlinear thermal expansion coefficients due to temperature and Λ_3 and Λ_4 are linear and nonlinear thermal expansion coefficients due to concentration, ρ_f is density of base liquid, c_p is specific heat capacity of the base fluid, α_f is thermal diffusivity of the base fluid, T is temperature, C is concentration, σ is electric conductivity, B_0^2 is magnetic parameter, k_1 is a reaction rate, D_B is the Brownian diffusion coefficient, D_T is the thermophoresis diffusion coefficient, and τ is the ratio of the effective heat capacity of the nanoparticle material and the heat capacity of base fluid.

These simultaneous partial differential equations (PDEs) (3)-(6) with the corresponding boundary conditions (7) are reduced to ordinary differential equations (ODEs) using similarity transformation. In this case, continuity equation and momentum equation are reduced to a single ODE and energy equation and concentration equation are reduced to another ODE.

We know set up the similarity transformation as follows [31]:

$$\eta = y\sqrt{\frac{a(n+1)}{2\nu}}x^{(n-1)/2},$$

$$v = -\sqrt{\frac{a\nu(n+1)}{2}}x^{(n-1)/2}\left[f(\eta) + \left(\frac{n-1}{n+1}\right)\eta f'(\eta)\right]$$

$$u = ax^n f'(\eta),$$

$$\psi = \sqrt{\frac{2\nu a}{n+1}} x^{(n+1)/2} f(\eta),$$
$$\theta(\eta) = \frac{T - T_\infty}{T_w - T_\infty}$$
$$\text{and } \phi(\eta) = \frac{C - C_\infty}{C_w - C_\infty}, \tag{8}$$

where η is a similarity variable ψ stream function defined as $u = \partial\psi/\partial y$ and $v = \partial\psi/\partial x$ which identically satisfies continuity equation (3), f is dimensionless function, θ is dimensionless temperature, and ϕ is dimensionless nanoparticle concentration.

Substituting (8) into (4)-(6), we obtain the following corresponding simultaneous nonlinear ordinary differential equations:

$$ff'' - \frac{2n}{n+1} f'^2 + (1+\varepsilon) f''' - \varepsilon\delta \left(\frac{n+1}{2}\right) f''^2 f''' - \frac{2}{n+1} M f' + \frac{2\lambda}{n+1} (1 + \beta_t \theta)\theta + \frac{2\lambda}{n+1} N^* (1 + \beta_c \phi)\phi = 0 \tag{9}$$

$$\theta'' + \Pr f\theta' + \Pr \gamma_E \left(\frac{n-3}{2} ff'\theta' - \frac{n+1}{2} f^2\theta''\right) + \frac{2}{n+1} \Pr \beta\theta + \Pr Nb\theta'\phi' + \Pr Nt\theta'^2 = 0 \tag{10}$$

$$\phi'' + \Pr Lef\phi' + \Pr Le\gamma_c \left(\frac{n-3}{2} ff'\phi' - \frac{n+1}{2} f^2\phi''\right) + \frac{Nt}{Nb}\theta'' - \frac{2}{n+1} \Pr Le\beta_1\phi = 0 \tag{11}$$

with the corresponding boundary conditions

$$\begin{aligned} f &= 0, \\ f' &= 1 \\ &\text{at } \eta = 0, \\ f' &\longrightarrow 0 \quad \text{as } \eta \longrightarrow \infty \\ \theta &= 1 \quad \text{at } \eta = 0, \\ \theta &\longrightarrow 0 \quad \text{as } \eta \longrightarrow \infty \\ \phi &= 1 \quad \text{at } \eta = 0, \\ \phi &\longrightarrow 0 \quad \text{as } \eta \longrightarrow \infty, \end{aligned} \tag{12}$$

where

$$\Pr = \frac{\nu_f}{\alpha_f},$$
$$\gamma_E = \lambda_E a x^{n-1},$$
$$\gamma_C = \lambda_C a x^{n-1},$$
$$\varepsilon = \frac{1}{\mu\beta^* c^*},$$
$$\delta = \frac{a^3 x^{3n-1}}{2\nu c^{*2}},$$
$$M = \frac{\sigma B_0^2}{x^{n-1} a \rho_f},$$
$$\lambda = \frac{Gr}{R_{ex}^2},$$
$$\beta_t = \frac{\Lambda_2}{\Lambda_1}(T_w - T_\infty),$$
$$\beta_c = \frac{\Lambda_4}{\Lambda_3}(C_w - C_\infty),$$
$$N^* = \frac{Gr^*}{Gr} = \frac{\Lambda_4}{\Lambda_3}\left(\frac{C_w - C_\infty}{T_w - T_\infty}\right),$$
$$Gr = \frac{g\Lambda_1}{\nu^2}(T_w - T_\infty) x^3,$$
$$Gr^* = \frac{g\Lambda 3}{\nu^2}(C_w - C_\infty) x^3,$$
$$Nb = \frac{D_B \tau (C_w - C_\infty)}{\nu},$$
$$Nb = \frac{D_T \tau (T_w - T_\infty)}{T_\infty \nu},$$
$$\beta = \frac{Q}{a x^{n-1} (\rho c_p)_f},$$
$$Le = \frac{\alpha_f}{D_B},$$
$$\beta_1 = \frac{k}{a}, \tag{13}$$

where Pr is the Prandtl number, γ_E is the Deborah number with respect to the relaxation time of the heat flux, γ_C is the Deborah number due to nanoparticle concentration, ε and δ are Eyring-Powell fluid parameters, M is magnetic field parameter, λ is mixed convection parameter/local buoyancy parameter, β_t is nonlinear convection parameter due to temperature, β_c is nonlinear convection parameter due to concentration, N^* is ratio of concentration to thermal buoyancy forces, Gr is Grashof number in terms of temperature, Gr^* is Grashof number in terms of concentration, Nb is Brownian motion parameter, Nt is thermophoresis parameter, β is heat generation/absorption term, Le is Lewis number, and β_1 is chemical reaction rate.

The Engineering quantities of interest in the study are local skin coefficient friction C_f, the Nusselt number Nu_x

and the nanoparticle of Sherwood number Sh_x are given by $C_f = \tau_w/\rho u_w^2, Nu_x = xq_w/k(T_w - T_\infty), Sh_x = xq_{np}/D_B(C_w - C_\infty)$, where τ_w is the wall skin friction, q_w is the heat flux and q_{np} is the nanofluid mass flux at the surface of the sheet defined as follow:

$$\tau_w = \left(\mu + \frac{1}{\beta C}\right)\frac{\partial u}{\partial y} - \frac{1}{6}\left(\frac{1}{C}\frac{\partial u}{\partial y}\right)^3,$$
$$q_w = -k\left(\frac{\partial T}{\partial y}\right)_{y=0}, \tag{14}$$
$$q_{np} = -D_B\left(\frac{\partial \phi}{\partial y}\right)_{y=0}.$$

After replacing the values from similarity transformation in (8) into (14), we obtain

$$\mathrm{Re}_x^{1/2} C_f = \sqrt{\frac{n+1}{2}}\left[(1+\varepsilon) f''(0) - \frac{\varepsilon\delta}{3}\left(f''(0)\right)^3\right],$$
$$Nu_r = \frac{Nu_x}{\left(((n+1)/2)\,\mathrm{Re}_x\right)^{1/2}} = -\theta'(0) \tag{15}$$
$$\text{and } \mathrm{Sh}_r = \frac{Sh_x}{\left(((n+1)/2)\,\mathrm{Re}_x\right)^{1/2}} = -\phi'(0).$$

Here, N_{ur} and Sh_r are reduced form of Nusselt number and nanoparticle Sherwood number, respectively, and the local Reynolds number depending on the nonlinear stretching surface velocity is given by

$$\mathrm{Re}_x = \frac{u_x x}{\nu}. \tag{16}$$

3. Method of Solution

We employed the Galerkin finite element method which is a prominent technique to solve nonlinear differential equations through the following five steps that are essential to realize what the approach of the FEM is (see [13, 32–34]):

(i) Discretization of the domain into elements

(ii) Element formulation which is called setup of differential equation in its weak form

(iii) Assembly of element equations known as setup of global problem or obtaining equations for the entire system from the equations for one element

(iv) Impose the appropriate boundary condition

(v) Solve the system of equations.

An attribute feature of the finite element method is that, instead of seeking the approximation solution over the entire region, the region is partitioned into smaller elements and the approximation is then carried out over each element. After determining the character of all single elements, the elements is patched together, which hopefully enables us to get an approximate solution over the entire body.

Assuming

$$f' = g \tag{17}$$

the simultaneous nonlinear ordinary differential equations in (9)-(11) with the boundary conditions in (12) are reduced to

$$fg' - \frac{2n}{n+1}g^2 + (1+\varepsilon)g'' - \varepsilon\delta\left(\frac{n+1}{2}\right)g'^2 g'' - \frac{2}{n+1}Mg + \frac{2\lambda}{n+1}(1+\beta_t\theta)\theta + \frac{2\lambda}{n+1}N^*(1+\beta_c\phi)\phi = 0 \tag{18}$$

$$\theta'' + \mathrm{Pr}\, f\theta' + \mathrm{Pr}\,\gamma_E\left(\frac{n-3}{2}fg\theta' - \frac{n+1}{2}f^2\theta''\right) + \frac{2}{n+1}\mathrm{Pr}\,\beta\theta + \mathrm{Pr}\,Nb\theta'\phi' + \mathrm{Pr}\,Nt\theta'^2 = 0 \tag{19}$$

$$\phi'' + \mathrm{Pr}\,Lef\phi' + \mathrm{Pr}\,Le\gamma_c\left(\frac{n-3}{2}fg\phi' - \frac{n+1}{2}f^2\phi''\right) + \frac{Nt}{Nb}\theta'' - \frac{2}{n+1}\mathrm{Pr}\,Le\beta_1\phi = 0, \tag{20}$$

with the corresponding boundary conditions

$$\begin{aligned} &f = 0,\\ &g = 1 \\ &\qquad \text{at } \eta = 0,\\ &g \longrightarrow 0 \quad \text{as } \eta \longrightarrow \infty\\ &\theta = 1 \quad \text{at } \eta = 0,\\ &\theta \longrightarrow 0 \quad \text{as } \eta \longrightarrow \infty\\ &\phi = 1 \quad \text{at } \eta = 0,\\ &\phi \longrightarrow 0 \quad \text{as } \eta \longrightarrow \infty. \end{aligned} \tag{21}$$

At this step, we discretize the whole domain into elements called Mesh.

The second step is writing the weighted integral form associated with (17), (18), (19), and (20) over a typical three-node linear element (η_e, η_{e+1}) as follows:

$$\int_{\eta_e}^{\eta_{e+1}} w_1\left\{f' - g\right\}d\eta = 0 \tag{22}$$

$$\int_{\eta_e}^{\eta_{e+1}} w_2\left\{fg' - \frac{2n}{n+1}g^2 + (1+\varepsilon)g'' - \varepsilon\delta\left(\frac{n+1}{2}\right)g'^2 g'' - \frac{2}{n+1}Mg + \frac{2\lambda}{n+1}(1+\beta_t\theta)\theta + \frac{2\lambda}{n+1}N^*(1+\beta_c\phi)\phi\right\}d\eta = 0 \tag{23}$$

$$\int_{\eta_e}^{\eta_{e+1}} w_3 \left\{\theta'' + \Pr f\theta' + \Pr \gamma_E \left(\frac{n-3}{2} fg\theta' - \frac{n+1}{2} f^2\theta''\right) + \frac{2}{n+1} \Pr \beta\theta + \Pr Nb\theta'\phi' + \Pr Nt\theta'^2\right\} d\eta = 0 \quad (24)$$

$$\int_{\eta_e}^{\eta_{e+1}} w_4 \left\{\phi'' + \Pr Lef\phi' + \Pr Le\gamma_C \left(\frac{n-3}{2} fg\phi' - \frac{n+1}{2} f^2\phi''\right) + \frac{Nt}{Nb}\theta'' - \frac{2}{n+1} \Pr Le\beta_1\phi\right\} d\eta = 0, \quad (25)$$

where w_1, w_2, w_3, and w_4 are arbitrary weight functions and may be considered as the variation in f, g, θ, and ϕ, respectively, and domain (η_e, η_{e+1}) represents the interval of the boundary layer region.

At the third step, we seek approximation solution of the form

$$\begin{aligned} f &= \sum_{j=1}^{3} f_j\psi_j, \\ g &= \sum_{j=1}^{3} g_j\psi_j, \\ \theta &= \sum_{j=1}^{3} \theta_j\psi_j, \\ \phi &= \sum_{j=1}^{3} \phi_j\psi_j \end{aligned} \quad (26)$$

with $w_1 = w_2 = w_3 = w_4 = \psi_i$ $(i = 1, 2, 3)$, the quadratic shape functions ψ_i defined as

$$\begin{aligned} \psi_1^e &= \frac{(\eta_{e+1} - \eta)(\eta_{e+1} + \eta_e - 2\eta)}{(\eta_{e+1} - \eta_e)^2}, \\ \psi_2^e &= \frac{4(\eta - \eta_e)(\eta_{e+1} - \eta)}{(\eta_{e+1} - \eta_e)^2}, \\ \psi_3^e &= -\frac{(\eta - \eta_e)(\eta_{e+1} + \eta_e - 2\eta)}{(\eta_{e+1} - \eta_e)^2}, \end{aligned} \quad (27)$$

where $\eta_e \le \eta \le \eta_{e+1}$

At the fourth step, replacing approximate solution (26) into (22)-(25), we obtain the finite element model for the equation which is given by

$$[K^e][Y^e] = [F^e], \quad (28)$$

where $[K^e]$ denotes the elemental stiffness matrix, $[Y^e]$ is the vector of elemental nodal variables (unknowns), and $[F^e]$ is the force vector expressed as follows:

$$[K^e] = \begin{bmatrix} [K^{11}] & [K^{12}] & [K^{13}] & [K^{14}] \\ [K^{21}] & [K^{22}] & [K^{23}] & [K^{24}] \\ [K^{31}] & [K^{32}] & [K^{33}] & [K^{34}] \\ [K^{41}] & [K^{42}] & [K^{43}] & [K^{44}] \end{bmatrix},$$

$$[Y^e] = \begin{bmatrix} \{f\} \\ \{g\} \\ \{\theta\} \\ \{\phi\} \end{bmatrix}, \quad (29)$$

$$[F^e] = \begin{bmatrix} \{h^1\} \\ \{h^2\} \\ \{h^3\} \\ \{h^4\} \end{bmatrix},$$

where each $[K^{mn}]$ is of the order $3x3$ and $[h^m], (m, n = 1, 2.3, 4)$ is of the order $3x1$.

These matrices are defined as

$$\begin{aligned} K_{ij}^{11} &= \int_{\eta_e}^{\eta_{e+1}} \psi_i \frac{\partial\psi_j}{\partial\eta} d\eta, \\ K_{ij}^{12} &= -\int_{\eta_e}^{\eta_{e+1}} \psi_i\psi_j d\eta, \\ K_{ij}^{13} &= 0, \\ K_{ij}^{14} &= 0, \\ \mathrm{K}_{\mathrm{ij}}^{21} &= 0 \\ K_{ij}^{22} &= \int_{\eta_e}^{\eta_{e+1}} \psi_i \overline{f} \frac{\partial\psi_j}{\partial\eta} d\eta - \frac{2n}{n+1} \int_{\eta_e}^{\eta_{e+1}} \psi_i \overline{g} \psi_j d\eta \\ &\quad - (1+\varepsilon) \int_{\eta_e}^{\eta_{e+1}} \frac{\partial\psi_i}{\partial\eta} \frac{\partial\psi_j}{\partial\eta} d\eta \\ &\quad - \varepsilon\delta \frac{n+1}{2} \int_{\eta_e}^{\eta_{e+1}} \psi_i \overline{g'}\, \overline{g''} \frac{\partial\psi_j}{\partial\eta} d\eta \\ &\quad - \frac{2}{n+1} M \int_{\eta_e}^{\eta_{e+1}} \psi_i\psi_j d\eta, \\ K_{ij}^{23} &= \frac{2\lambda}{n+1} \int_{\eta_e}^{\eta_{e+1}} \psi_i\psi_j d\eta + \frac{2\lambda}{n+1} \beta_t \int_{\eta_e}^{\eta_{e+1}} \psi_i \overline{\theta} \psi_j d\eta \\ K_{ij}^{24} &= \frac{2\lambda}{n+1} N^* \int_{\eta_e}^{\eta_{e+1}} \psi_i\psi_j d\eta \\ &\quad + \frac{2\lambda}{n+1} N^* \beta_c \int_{\eta_e}^{\eta_{e+1}} \psi_i \overline{\phi} \psi_j d\eta, \end{aligned}$$

$$
\begin{aligned}
K_{ij}^{31} &= 0,\\
K_{ij}^{32} &= 0,\\
K_{ij}^{33} &= -\int_{\eta_e}^{\eta_{e+1}} \frac{\partial \psi_i}{\partial \eta}\frac{\partial \psi_j}{\partial \eta}d\eta + \Pr\int_{\eta_e}^{\eta_{e+1}} \psi_i \overline{f}\frac{\partial \psi_j}{\partial \eta}d\eta\\
&\quad + \Pr\gamma_E \frac{n-3}{2}\int_{\eta_e}^{\eta_{e+1}} \psi_i \overline{f}\,\overline{g}\frac{\partial \psi_j}{\partial \eta}d\eta\\
&\quad - \Pr\gamma_E \frac{n+1}{2}\int_{\eta_e}^{\eta_{e+1}} \psi_i \overline{f}\,\overline{f}\frac{\partial^2 \psi_j}{\partial \eta^2}d\eta\\
&\quad + \frac{2}{n+1}\Pr\beta\int_{\eta_e}^{\eta_{e+1}} \psi_i\psi_j d\eta\\
&\quad + \Pr Nb\int_{\eta_e}^{\eta_{e+1}} \psi_i \overline{\phi'}\frac{\partial \psi_j}{\partial \eta}d\eta\\
&\quad + \Pr Nt\int_{\eta_e}^{\eta_{e+1}} \psi_i \overline{\theta'}\frac{\partial \psi_j}{\partial \eta}d\eta,\\
K_{ij}^{34} &= 0,\\
K_{ij}^{41} &= 0,\\
K_{ij}^{42} &= 0\\
K_{ij}^{43} &= -\frac{Nt}{Nb}\int_{\eta_e}^{\eta_{e+1}} \frac{\partial \psi_i}{\partial \eta}\frac{\partial \psi_i}{\partial \eta}d\eta,\\
K_{ij}^{44} &= -\int_{\eta_e}^{\eta_{e+1}} \frac{\partial \psi_i}{\partial \eta}\frac{\partial \psi_i}{\partial \eta}d\eta + \Pr Le\int_{\eta_e}^{\eta_{e+1}} \psi_i \overline{f}\frac{\partial \psi_i}{\partial \eta}d\eta\\
&\quad + \Pr Le\gamma_C \frac{n-3}{2}\int_{\eta_e}^{\eta_{e+1}} \psi_i \overline{f}\,\overline{g}\frac{\partial \psi_j}{\partial \eta}d\eta\\
&\quad - \Pr Le\gamma_C \frac{n+1}{2}\int_{\eta_e}^{\eta_{e+1}} \psi_i \overline{f}\,\overline{f}\frac{\partial^2 \psi_j}{\partial \eta^2}d\eta\\
&\quad - \frac{2}{n+1}\Pr Le\beta_1\int_{\eta_e}^{\eta_{e+1}} \psi_i\psi_j d\eta\\
h_i^1 &= 0,\\
h_i^2 &= -(1+\varepsilon)\left(\psi_i\frac{\partial g}{\partial \eta}\right)_{\eta_e}^{\eta_{e+1}},\\
h_i^3 &= -\left(\psi_i\frac{\partial \theta}{\partial \eta}\right)_{\eta_e}^{\eta_{e+1}},\\
h_i^4 &= -\left(\psi_i\frac{\partial \phi}{\partial \eta} + \frac{Nt}{Nb}\psi_i\frac{\partial \theta}{\partial \eta}\right)_{\eta_e}^{\eta_{e+1}},
\end{aligned}
\tag{30}
$$

where

$$
\begin{aligned}
\overline{f}' &= \sum_{j=1}^{3}\overline{f}_j\frac{\partial \psi_j}{\partial \eta},\\
\overline{g'} &= \sum_{j=1}^{3}\overline{g_j}\frac{\partial \psi_j}{\partial \eta},\\
\overline{\theta'} &= \sum_{j=1}^{3}\overline{\theta}_j\frac{\partial \psi_j}{\partial \eta},\\
\overline{\phi'} &= \sum_{j=1}^{3}\overline{\phi}_j\frac{\partial \psi_j}{\partial \eta}.
\end{aligned}
\tag{31}
$$

4. Results and Discussion

The numerical method employed to solve the present problem is influential method in solving nonlinear partial differential equations and called Galerkin finite element method (GFEM). The nonlinear partial differential equations governing the laminar boundary layer flow were converted to the matching nonlinear ordinary differential equations (ODEs) using appropriate similarity transformation and then passed through five necessary steps for solving differential equations using GFEM. We used Gaussian integration rule to evaluate the integrations in (30) and (31) and Matlab software is employed to produce the numerical result. Moreover, we interpreted the impact of physical parameters like magnetic field, Prandtl number, Brownian motion, thermophoresis, mixed convection/local buoyancy parameter, Deborah number with respect to the relaxation time of the heat flux and nanoparticle concentration, heat generation or absorption term, chemical reaction rate, ratio of concentration to thermal buoyancy forces, and stretching sheet parameter. The results are illustrated by tabular and graphical forms. The default values of the related parameters used for this study are

$$
\begin{aligned}
\Pr &= 1.0,\\
\lambda &= 0.2,\\
\varepsilon &= 0.3,\\
\beta_1 &= 0.3,\\
\delta &= 0.2,\\
\gamma_E &= 0.2,\\
\gamma_C &= 0.2,\\
n &= 1.2,\\
M &= 1.0,\\
Nt &= 0.1,\\
Nb &= 0.1,
\end{aligned}
$$

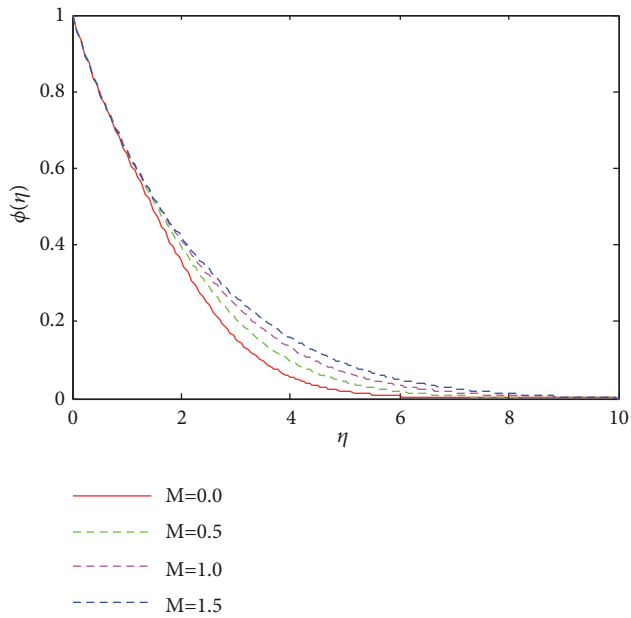

Figure 2: Impact of magnetic parameter M on nanoparticle concentration.

$$N^* = 0.1,$$
$$\beta_t = 0.3,$$
$$Le = 1.0,$$
$$\beta = 0.1,$$
$$\beta_c = 0.2. \tag{32}$$

These values are carefully chosen in accordance with previous literatures (see [31]).

Figures 2, 3, and 4 show the impacts of magnetic field variable on nanoparticle concentration, temperature profile, and velocity field, respectively. Figures 2 and 3 show the attribute of both nanoparticle concentration and temperature profile of the fluid when magnetic field varies. The graphs reveal that as magnetic field intensified, both the temperature and concentration graphs rise up. This is in agreement with the physical meanings of magnetic field which is directly related to Lorentz force that has the capability of increasing the nanoparticle volume fraction in the motion of the nanofluid and fluid temperature as well. Opposite to this as seen from Figure 4, the enhancement in magnetic field parameter reduces the fluid velocity. This is due to the enhancement of Lorentz force which opposes the motion of the fluid.

It is observed from Figure 6 that an increase in thermophoresis parameter increases the temperature of the fluid. This is a result of large thermophoretic force which causes large temperature gradient that produces movement of suspended particle from higher temperature to lower temperature.

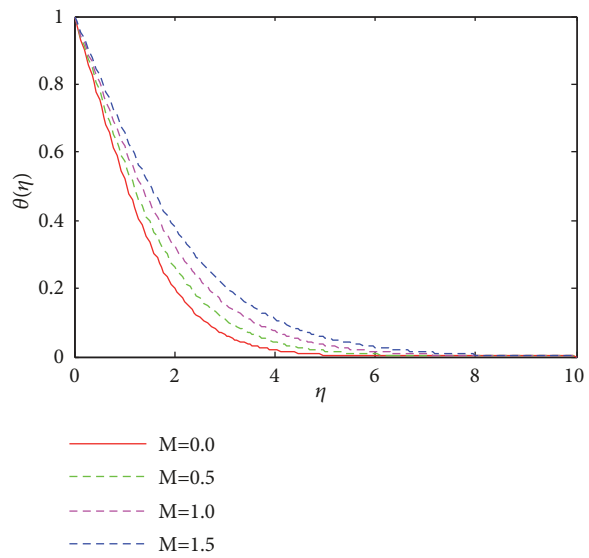

Figure 3: Impact of magnetic parameter M on temperature profile.

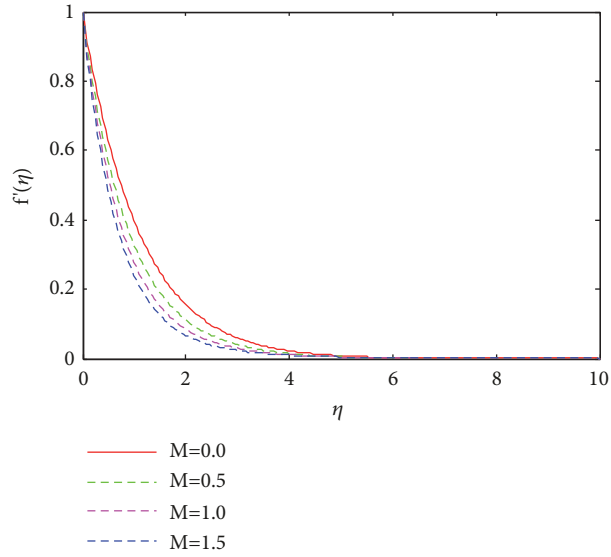

Figure 4: Impact of magnetic parameter M on velocity field.

Figures 5 and 7 also indicate that the enhancement in thermophoresis parameter will enhance both velocity of the fluid and nanoparticle concentration profile. This is due to large thermophoresis which causes particle migration to produce nonuniform distribution of nanoparticle concentration as seen from Figure 7.

Brownian motion is the unsystematic motion of particles suspended in fluid resulting from their collision with high-speed moving molecules in the fluid. It is crystal clear that Brownian motion parameter enlargement leads to the increase in thermal boundary layer region as indicated in Figure 9 and opposite to this the enlargement in Brownian motion parameter which causes in fluid motion the particle deposition away from fluid regime and then produces the

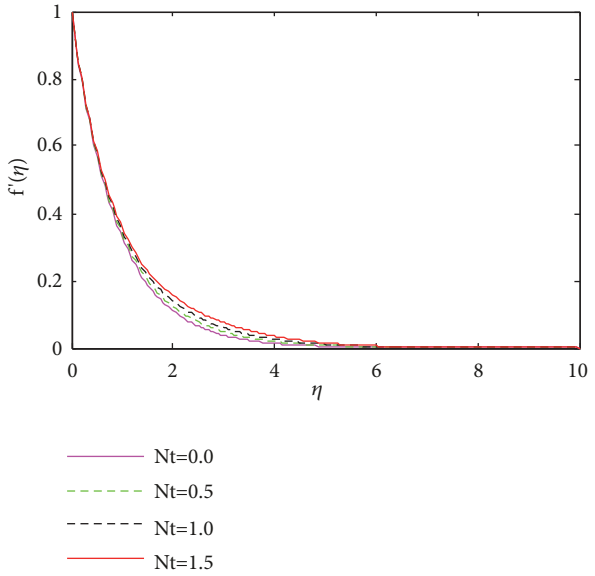

Figure 5: Impact of thermophoresis Nt on velocity field.

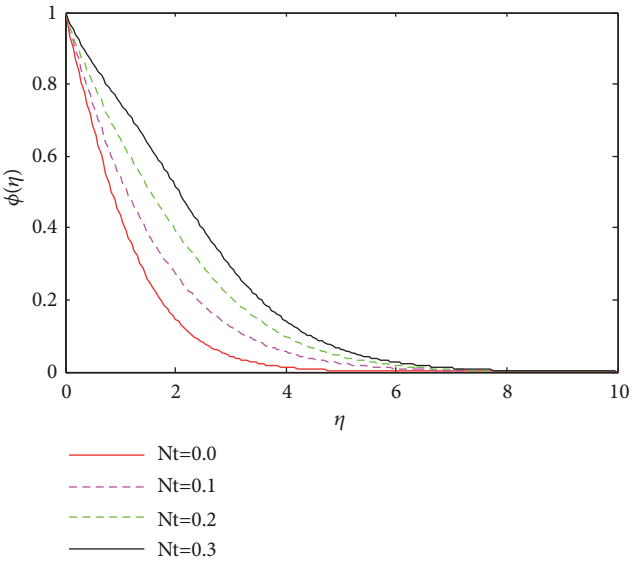

Figure 7: Impact of thermophoresis Nt on nanoparticle concentration.

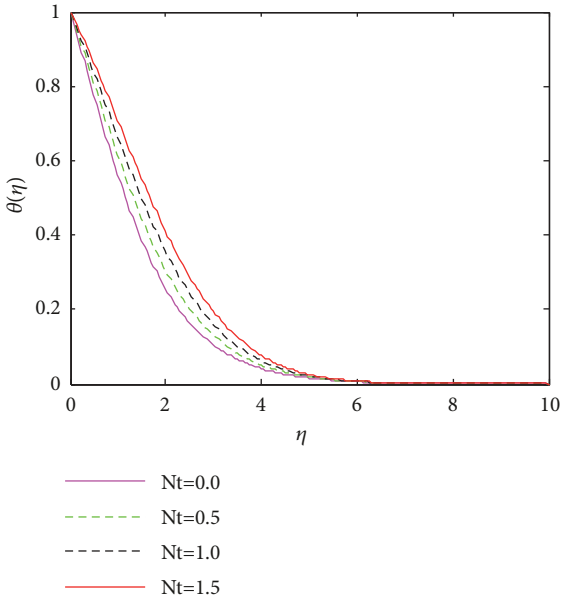

Figure 6: Impact of thermophoresis Nt on temperature profile.

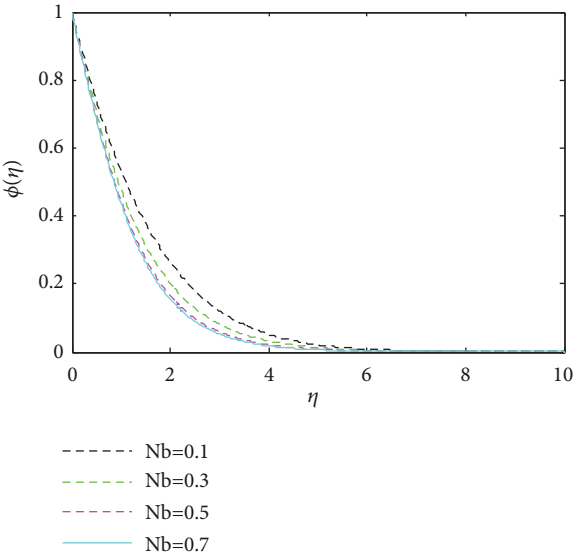

Figure 8: Impact of Brownian motion Nb on nanoparticle concentration.

nanoparticle volume fraction decrease or nanoparticle concentration reduction as shown in Figure 8.

Figure 10 reveals that the increase in heat generation or absorption parameter magnifies the temperature of the fluid and thermal boundary layer thickness of the fluid. This is simply as expected that adding heat to the fluid will rise temperature of the fluid. Figure 11 shows nanoparticle concentration diminishes as Lewis number increases. The Lewis number (Le) characterizes fluid flows where there are simultaneous heat and mass transfer. Thus, it is a measure of the relative thermal and mass-transfer (concentration) boundary layer thicknesses and hence increase in Lewis number also results in diminishing concentration boundary layer thickness.

Figures 12 and 13 describe the notion that the amplification in Prandtl number results in diminishing both temperature and nanoparticle concentration profile, respectively. It also indicates a shrink in both thermal boundary layer and boundary layer width of concentration. Since Prandtl number itself relates momentum diffusivity and thermal diffusivity, it controls the relative thickness of the momentum and thermal boundary layers. Therefore, a large value of Pr implies heat diffuses slowly compared to the velocity (momentum).

Figures 14–19 show mixed convection parameter λ and Eyring-Powell fluid parameter ε have similar influences on

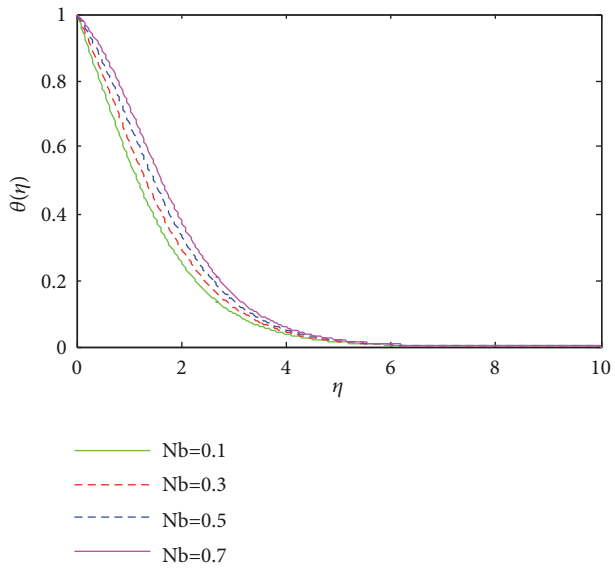

Figure 9: Impact of Brownian motion Nb on temperature profile.

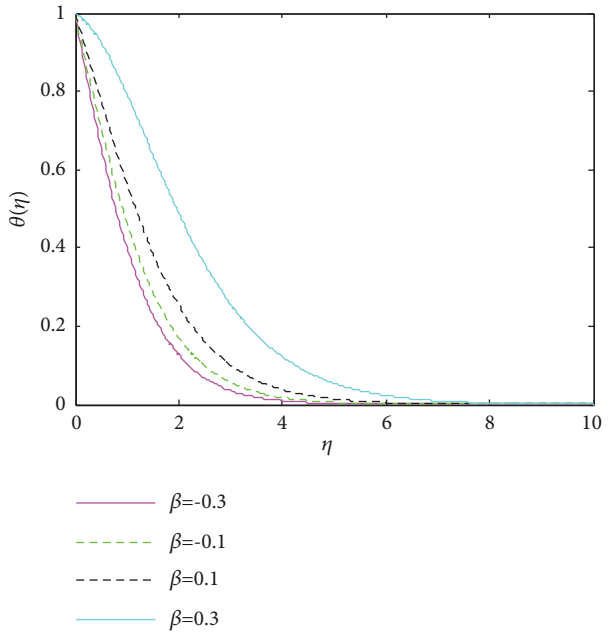

Figure 10: Impact of heat generation/absorption β on temperature profile.

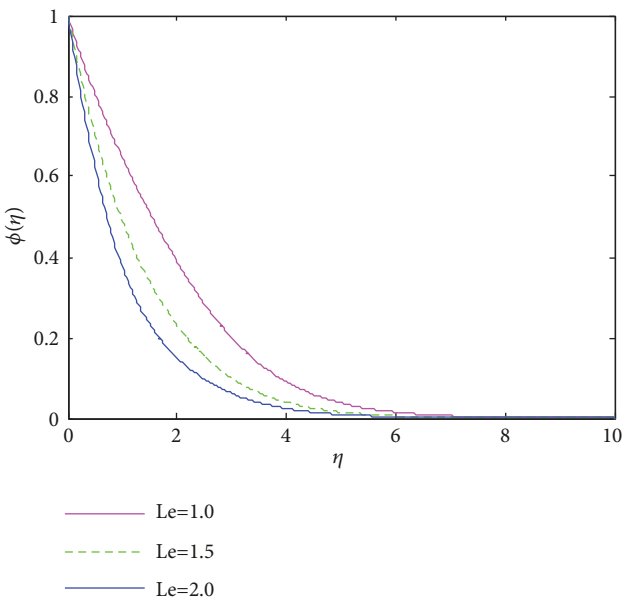

Figure 11: Impact of Lewis number Le on nanoparticle concentration.

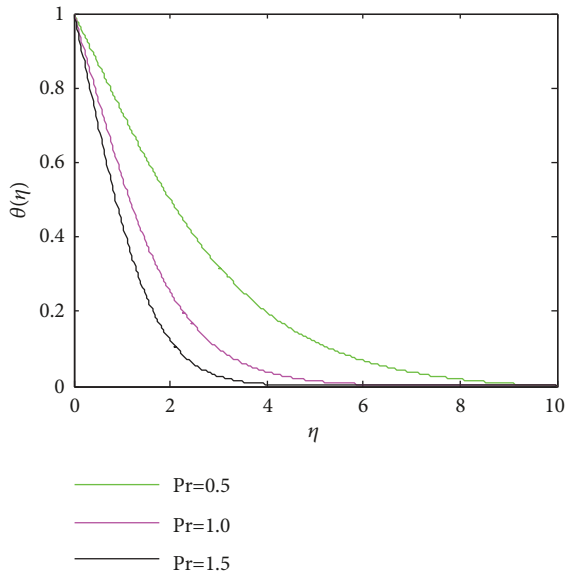

Figure 12: Impact of Prandtl number Pr on temperature profile.

velocity field, temperature, and nanoparticle concentration, respectively. Velocity field increases with enlargement in mixed convection parameter λ and both nanoparticle concentration and temperature of the fluid decrease with increase in λ. Eyring-Powell fluid parameter ε also exhibits similar property as shown in Figures 16–19.

As revealed in Figures 21 and 22, increase in chemical reaction rate β_1 reduces nanoparticle concentration; enhancement in Deborah number γ_E diminishes temperature profile and large values of Deborah number γ_C result in smaller value in nanoparticle concentration, respectively.

Figures 23 and 24 are drawn to manifest the effect of stretching sheet parameter on temperature and nanoparticle concentration profile, respectively. Stretching sheet parameter has decreasing impact on both temperature and nanoparticle concentration of the boundary layer flow.

Tables 1–3 pointed out that the results obtained in the present study in terms of engineering physical quantities of interest like local skin friction coefficient, local Nusselt number, and local Sheer wood number are in a good conformity with existing literature.

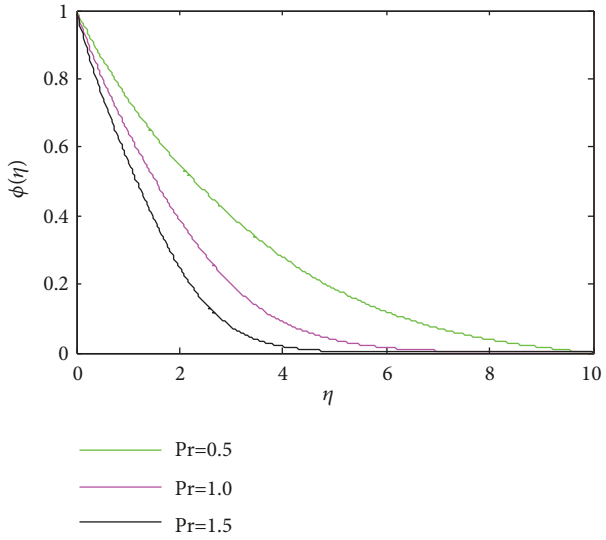

FIGURE 13: Impact of Prandtl number Pr on nanoparticle concentration profile.

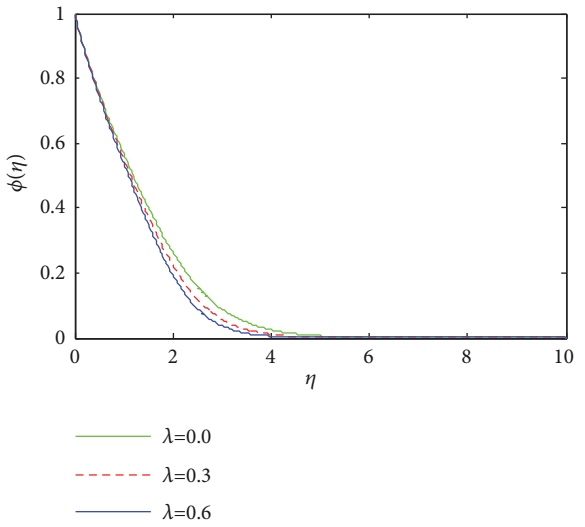

FIGURE 15: Impact of mixed convection parameter λ on nanoparticle concentration.

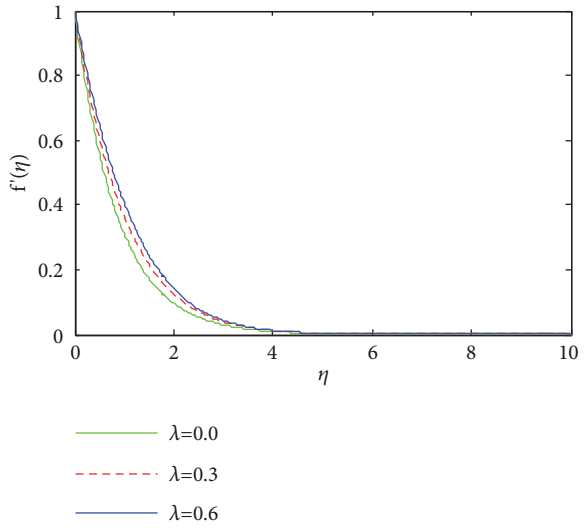

FIGURE 14: Impact of mixed convection parameter λ on velocity field.

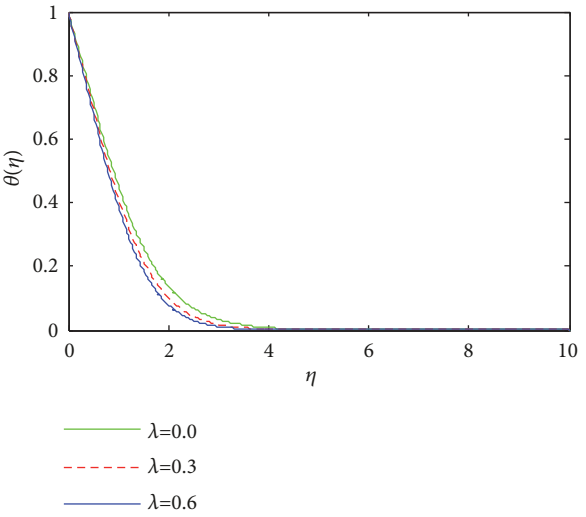

FIGURE 16: Impact of mixed convection parameter λ on temperature profile.

Table 4 reveals that the skin friction coefficient is an increasing function of magnetic field parameter M, stretching sheet parameter n, and Eyring-Powell fluid parameter ε and is a decreasing function of mixed convection parameter λ, and Eyring-Powell fluid parameter δ. Table 4 also indicates that local Nusselt number is an increasing function of Prandtl number Pr, Deborah number γ_E, mixed convection parameter λ, stretching sheet parameter n, and Eyring-Powell fluid parameters and is a decreasing function of Deborah number γ_C, heat generation or absorption term β, thermophoresis parameter N_t, and Brownian diffusion parameter Nb.

Table 4 also shows sheer wood number is an increasing function of Prandtl number Pr, Deborah number γ_C, mixed convection parameter λ, Eyring-Powell fluid parameters, chemical reaction rate β_1, heat generation or absorption term β, Brownian diffusion parameter Nb, and Lewis number Le and is a decreasing function of Deborah number γ_E, stretching sheet parameter n, and thermophoresis parameter Nt.

5. Conclusion

We investigated the nonlinear convective flow of Eyring-Powell nanofluid using Catteneo-Christov heat and mass flux model over a nonlinear stretching surface in the presence of heat generation/absorption and chemical reaction. The Galerkin finite element method (GFEM) is used to solve the coupled highly nonlinear partial differential equations resulting from the problem formulation. The attributes of the

Table 1: Comparison of the Nusselt number $\theta'(0)$ when $n = 1.0$, Pr $= 10.0$, $Le = 1.0$, $\varepsilon = \beta_1 = \delta = \gamma_E = \gamma_C = M = \beta = \beta_t = \beta_c = \lambda = 0.0$.

	Nusselt number											
Nt	$Nb = 0.1$			$Nb = 0.2$			$Nb = 0.3$			$Nb = 0.4$		
	[35]	[36]	present	[35]	[36]	Present	[35]	[36]	present	[35]	[36]	present
0.1	0.9524	0.95244	0.95239	0.5056	0.50561	0.50557	0.2522	0.25218	0.25217	0.1194	0.11940	0.11940
0.2	0.6932	0.69318	0.69318	0.3654	0.36536	0.36536	0.1816	0.18159	0.18159	0.0859	0.08588	0.08590
0.3	0.5201	0.52025	0.52019	0.2731	0.27313	0.27313	0.1355	0.13564	0.13554	0.0641	0.06424	0.06409
0.4	0.4026	0.40260	0.40258	0.2110	0.21100	0.21101	0.1046	0.10461	0.10461	0.0495	0.04962	0.04946
0.5	0.3211	0.32105	0.32109	0.1681	0.16811	0.16812	0.0833	0.08342	0.08330	0.0394	0.03932	0.03939

Table 2: Comparison of the Sheer wood number $\phi'(0)$ when $n = 1.0$, Pr $= 10.0$, $Le = 1.0$, $\varepsilon = \beta_1 = \delta = \gamma_E = \gamma_C = M = \beta = \beta_t = \beta_c = \lambda = 0.0$.

	Sheer wood number											
Nt	$Nb = 0.1$			$Nb = 0.2$			$Nb = 0.3$			$Nb = 0.4$		
	[35]	[36]	present	[35]	[36]	Present	[35]	[36]	present	[35]	[36]	Present
0.1	2.1294	2.12949	2.12938	2.3819	2.38186	2.38190	2.4100	2.41009	2.41002	2.3997	2.39970	2.39966
0.2	2.2740	2.27401	2.27400	2.5152	2.51537	2.51521	2.5150	2.51501	2.51500	2.4807	2.48066	2.48072
0.3	2.5286	2.52855	2.52855	2.6555	2.65550	2.65550	2.6088	2.60876	2.60884	2.5486	2.54848	2.54860
0.4	2.7952	2.79520	2.79519	2.7818	2.78181	2.78178	2.6876	2.68758	2.68761	2.6038	2.60380	2.60380
0.5	3.0351	3.03511	3.03511	2.8883	2.88830	2.88830	2.7519	2.75190	2.75188	2.6483	2.64831	2.64831

Table 3: Comparison of the skin friction $f''(0)$ when $n = 1.0$, Pr $= 1.0$, $Le = 1.0$, $\beta_1 = \gamma_E = \gamma_C = \beta = \beta_t = \beta_c = 0.0$.

ε	λ	δ	M	$-f''(0)$ [31]	$-f''(0)$ present
0.1	0.1	0.1	0.5	1.2272	1.22720
0.2				1.2826	1.28261
0.3				1.3361	1.33566
0.1		0.5		1.2216	1.22158
	0.3			1.1152	1.11520
	0.5			1.0133	1.01330
	0.1	0.1		1.2271	1.22720
		0.3		1.2245	1.22445
		0.5		1.2217	1.22168

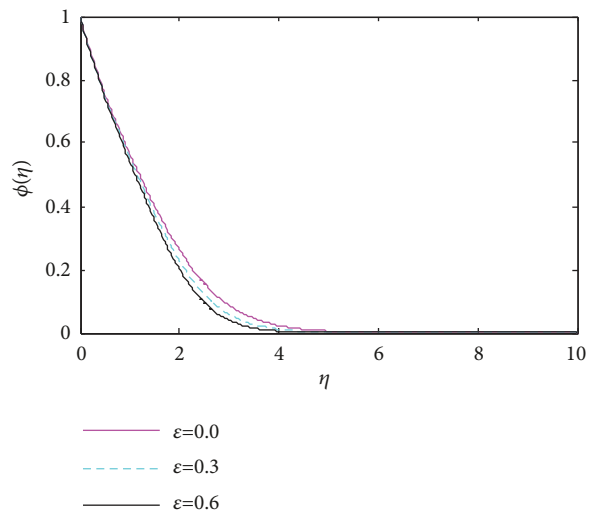

Figure 17: Impact of Eyring-Powell fluid parameter ε on nanoparticle concentration.

laminar follow pertinent to different governing parameters are indicated as follows:

(i) Both nanoparticle concentration and temperature of the fluid are increasing functions of the magnetic field parameter and the velocity field is decreasing function of the magnetic field parameter

(ii) Velocity field, temperature, and nanoparticle concentration profile are increasing functions of thermophoresis parameter

(iii) The enlargement in Brownian motion yields large values in temperature and decrease in nanoparticle concentration

(iv) Both nanoparticle concentration and temperature profile of the fluid are decreasing functions of the Lewis and Prandtl numbers

(v) The temperature and nanoparticle concentration are reduced and opposite to this the velocity

Table 4: Numerical values of skin friction coefficient, Nusselt number and Sheer wood number for different parameters.

n	Pr	λ	ε	β_1	δ	γ_E	γ_C	M	Nt	Nb	Le	β	$-f''(0)$	$-\theta'(0)$	$-\phi'(0)$
1.2	1.0	0.0	0.1	0.1	0.1	0.2	0.3	0.5	0.1	0.1	1.0	0.0	1.28652	0.53393	0.38052
	1.5												1.28652	0.66299	0.48308
	2.0												1.28652	0.76485	0.60785
	1.0	0.1											1.23845	0.54212	0.38183
		0.2											1.19147	0.54981	0.38327
		0.0	0.2										1.34109	0.54197	0.38170
			0.3										1.39448	0.54922	0.38300
			0.1	0.2									1.28652	0.53208	0.47720
				0.4									1.28652	0.52920	0.64069
				0.1	0.2								1.28175	0.53423	0.38054
					0.5								1.26850	0.53510	0.38060
					0.1	0.5							1.28652	0.55509	0.35871
						1.0							1.28652	0.61103	0.30691
						0.2	0.5						1.28652	0.53359	0.38194
							1.0						1.28652	0.39878	0.53207
							0.3	1.0					1.46343	0.50976	0.37836
								1.5					1.62013	0.49047	0.37790
								0.5	0.3				1.28652	0.49660	-0.09250
									0.5				1.28652	0.46138	-0.43839
									0.1	0.3			1.28652	0.47553	0.58955
										0.5			1.28652	0.42186	0.63049
										0.1	1.5		1.28652	0.52835	0.59337
											2.0		1.28652	0.52440	0.78393
											1.0	0.2	1.28652	0.34687	0.55032
												0.3	1.28652	0.22448	0.66179
												0.5	1.28652	-0.15594	1.01042
0.5	1.0	0.0	0.1	0.1	0.1	0.2	0.3	0.5	0.1	0.1	1.0	0.0	1.26147	0.51567	0.42594
1.5													1.29252	0.54171	0.36815
2.0													1.29941	0.55482	0.35257

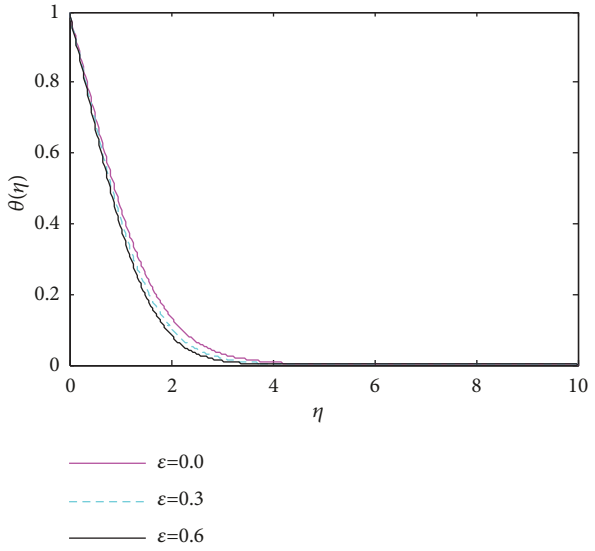

Figure 18: Impact of Eyring-Powell fluid parameter ε on temperature profile.

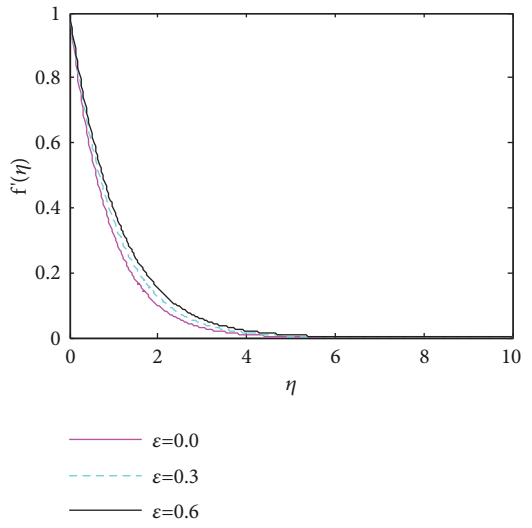

Figure 19: Impact of Eyring-Powell fluid parameter ε on velocity profile.

field increases when mixed convection parameter increases

(vi) Velocity field is increasing function of Eyring-Powell fluid parameter ε and both temperature and concentration profiles are decreasing functions of ε

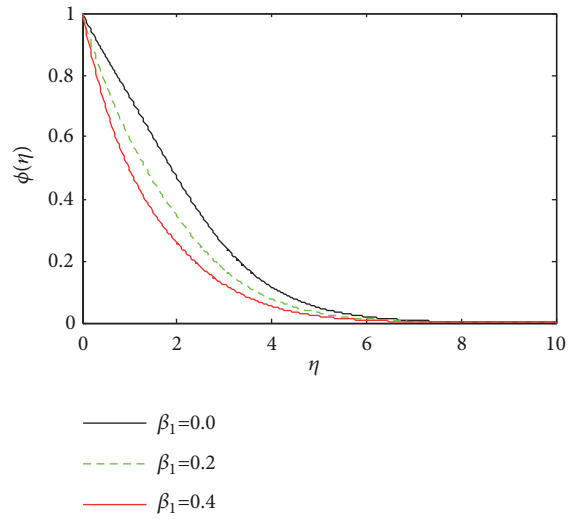

FIGURE 20: Impact of chemical reaction rate β_1 on nanoparticle concentration.

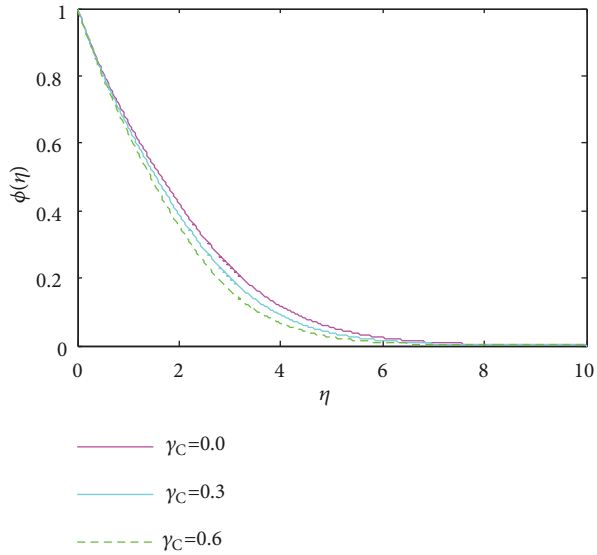

FIGURE 22: Impact of γ_C on nanoparticle concentration.

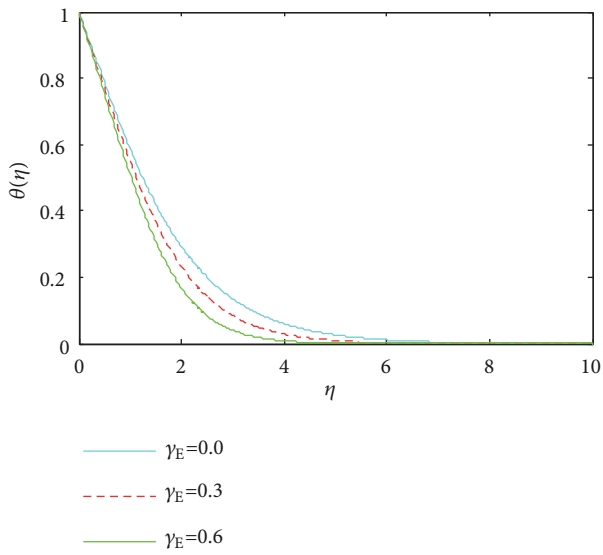

FIGURE 21: Impact of γ_E on temperature profile.

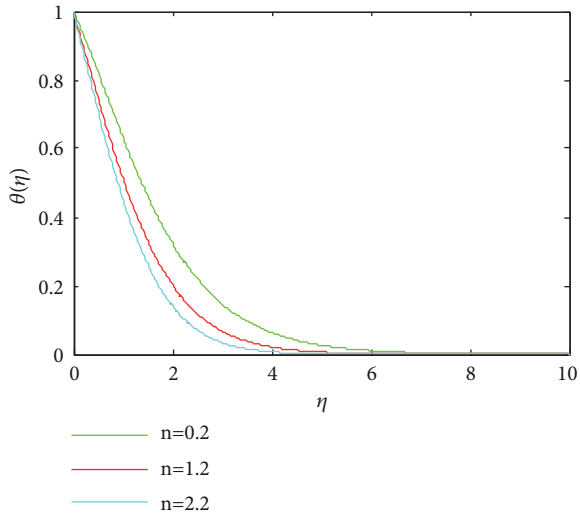

FIGURE 23: Impact of stretching sheet parameter n on temperature profile.

(vii) The rise in reaction rate β_1 and the Deborah number due to nanoparticle concentration γ_C diminishes nanoparticle concentration of the boundary layer flow

(viii) The larger stretching sheet parameter and the Deborah number with respect to relaxation time of heat flux γ_E results in reduction in temperature profile of the flowing fluid

(ix) The rise in chemical reaction rate will improve mass transfer rate and reduce heat transfer rate and local buoyancy parameter has quit opposite effect.

Nomenclature

a:	Constant
C:	Concentration
c_p:	Specific heat at constant pressure
C_f:	Skin friction coefficient
D_B:	Brownian diffusion
D_T:	Thermophoresis diffusion
$GFEM$:	Galerkin finite element method
T:	Temperature
g:	Gravitational acceleration
u, v:	Velocity components
U_w:	Stretching velocity
ν:	Kinematic viscosity
Λ_1, Λ_2:	Linear and nonlinear thermal expansion coefficients due to temperature

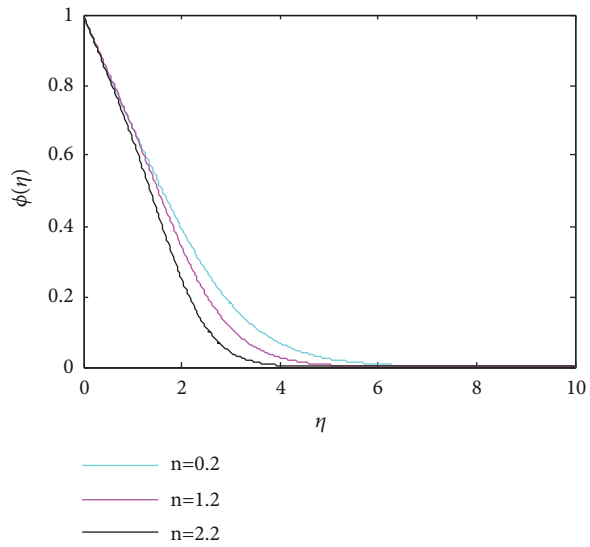

FIGURE 24: Impact of stretching sheet parameter n on nanoparticle concentration.

Λ_3, Λ_4: Linear and nonlinear thermal expansion coefficients due to concentration
ρ_f: Density of base liquid
α_f: Thermal diffusivity of the base fluid
σ: Electric conductivity
B_0^2: Magnetic field parameter
k_1: Reaction rate
Pr: Prandtl number
γ_E: Deborah number with respect to the relaxation time of the heat flux
γ_C: Deborah number due to nanoparticle concentration
ε, δ: Eyring-Powell fluid parameters
M: Magnetic field parameter
λ: Mixed convection parameter
β_t: Nonlinear convection parameter due to temperature
β_c: Nonlinear convection parameter due to concentration
N^*: Ratio of concentration to thermal buoyancy forces
Gr: Grashof number in terms of temperature
Gr^*: Grashof number in terms of concentration
N_b: Brownian motion parameter
N_t: Thermophoresis parameter
β: Heat generation/absorption term
Le: Lewis number
β_1: Chemical reaction rate parameter
N_{ux}: Nusselt number
Sh_x: Sherwood number subscript
∞: Condition at the free stream
w: Condition at the surface.

Data Availability

The data used in this article is freely available for the user.

Conflicts of Interest

The authors declare that they have no conflicts of interest.

References

[1] S. Panigrahi, M. Reza, and A. K. Mishra, "Mixed convective flow of a powell-eyring fluid over a non-linear stretching surface with thermal diffusion and diffusion thermo," *Procedia Engineering*, vol. 127, pp. 645–651, 2015.

[2] I. Khan, M. Qasim, and S. Shafie, "Flow of an Erying-Powell fluid over a stretching sheet in presence of chemical reaction," *Thermal Science International Scientific Journal*, vol. 20, pp. 1903–1912, 2016.

[3] S. Abdul Gaffar, V. E. Ramachandra Prasad, and K. Reddy, "Non-Newtonian thermal convection of Eyring-Powell fluid from an isothermal sphere with biot number effects," *International Journal of Industrial Mathematics*, vol. 8, no. 2, 2016.

[4] S. Alharbi, A. Dawar, Z. Shah et al., "Entropy generation in MHD eyring–powell fluid flow over an unsteady oscillatory porous stretching surface under the impact of thermal radiation and heat source/sink," *Applied Sciences*, vol. 8, no. 12, article 2588, 2018.

[5] B. Ahmad and Z. Iqbal, "An effect of Cattaneo Christov heat flux model for eyring powell fluid over an exponentially stretching sheet," *Frontiers in Heat and Mass Transfer*, vol. 8, no. 22, 2017.

[6] A. M. Megahed, "Variable viscosity and slip velocity effects on the flow and heat transfer of a power-law fluid over a non-linearly stretching surface with heat flux and thermal radiation," *Rheologica Acta*, vol. 51, no. 9, pp. 841–847, 2012.

[7] A. M. Megahed, "Flow and heat transfer of a non-Newtonian power-law fluid over a non-linearly stretching vertical surface with heat flux and thermal radiation," *Meccanica*, vol. 50, no. 7, pp. 1693–1700, 2015.

[8] A. M. Megahed, "Flow and heat transfer of non-Newtonian Sisko fluid past a nonlinearly stretching sheet with heat generation and viscous dissipation," *Journal of the Brazilian Society of Mechanical Sciences and Engineering*, vol. 40, no. 492, 2018.

[9] M. S. Upadhay, Mahesha, and C. S. K. Raju, "Cattaneo-Christov on heat and mass transfer of unsteady Eyring-Powell dusty nanofluid over sheet with heat and mass flux conditions," *Informatics in Medicine Unlocked*, vol. 9, pp. 76–85, 2017.

[10] K. Anantha Kumar, J. V. Ramana Reddy, V. Sugunamma, and N. Sandeep, "Magnetohydrodynamic Cattaneo-Christov flow past a cone and a wedge with variable heat source/sink," *Alexandria Engineering Journal*, vol. 571, pp. 435–443, 2016.

[11] A. Kumar, V. Sugunamma, and N. Sandeep, "Impact of non-linear radiation on mhd non-aligned stagnation point flow of micropolar fluid over a convective surface," *Journal of Non-Equilibrium Thermodynamics*, vol. 43, no. 4, pp. 327–345, 2018.

[12] K. Anantha Kumar, V. Sugunamma, N. Sandeep, and J. V. Ramana Reddy, "Impact of Brownianmotion and thermophoresis on bioconvective flow of nanoliquids past a variable thickness surface with slip effects," *Multidiscipline Modeling in Materials and Structures*, 2018.

[13] T. Hayat, R. Sajjad, T. Muhammad, A. Alsaedi, and R. Ellahi, "MHD nonlinear stretching flow of Powell–Eyring nanomaterial," *Results in Physics*, vol. 7, pp. 535–543, 2017.

[14] M. Madhu and N. Kishan, "MHD Boundary-layer flow of a non-Newtonian nanofluid Past a Stretching sheet with a heat source/sink," *Journal of Applied Mechanics and Technical Physics*, vol. 57, no. 5, pp. 908–915, 2016.

[15] J. Rahimi, D. D. Ganji, M. Khaki, and K. Hosseinzadeh, "Solution of the boundary layer flow of an Eyring-Powell non-Newtonian fluid over a linear stretching sheet by collocation method," *Alexandria Engineering Journal*, vol. 56, no. 4, pp. 621–627, 2017.

[16] A. T. Akinshilo and O. Olaye, "On the analysis of the Eyring Powell model based fluid flow in a pipe with temperature dependent viscosity and internal heat generation," *Journal of King Saud University - Engineering Sciences*, vol. 31, no. 3, pp. 271–279, 2019.

[17] M. Madhu and N. Kishan, "Finite element analysis of heat and mass transfer by MHD mixed convection stagnation-point flow of a non-Newtonian power-law nanofluid towards a stretching surface with radiation," *Journal of the Egyptian Mathematical Society*, vol. 24, no. 3, pp. 458–470, 2016.

[18] M. Jayachandra Babu, N. Sandeep, and S. Saleem, "Free convective MHD Cattaneo-Christov flow over three different geometries with thermophoresis and Brownian motion," *Alexandria Engineering Journal*, vol. 56, no. 4, pp. 659–669, 2017.

[19] K. Vajravelu and K. S. Sastri, "Fully developed laminar free convection flow between two parallel vertical walls-I," *International Journal of Heat and Mass Transfer*, vol. 20, no. 6, pp. 655–660, 1977.

[20] R. Bhargava and R. S. Agarwal, "Fully developed free convection flow in a circular pipe," *Indian Journal of Pure and Applied Mathematics*, vol. 10, pp. 357–365, 1979.

[21] M. I. Khan, S. Qayyum, T. Hayat, M. . Khan, A. Alsaedi, and T. A. Khan, "Entropy generation in radiative motion of tangent hyperbolic nanofluid in presence of activation energy and nonlinear mixed convection," *Physics Letters A*, vol. 382, no. 31, pp. 2017–2026, 2018.

[22] K. Vajravelu, J. R. Cannon, J. Leto et al., "Nonlinear convection at a porous flat plate with application to heat transfer from a dike," *Journal of Mathematical Analysis and Applications*, vol. 277, no. 2, pp. 609–623, 2003.

[23] M. I. Khan, M. Waqas, T. Hayat, M. I. Khan, and A. Alsaedi, "Numerical simulation of nonlinear thermal radiation and homogeneous-heterogeneous reactions in convective flow by a variable thicked surface," *Journal of Molecular Liquids*, vol. 246, pp. 259–267, 2017.

[24] T. Hayat and S. Nadeem, "Flow of 3D Eyring-Powell fluid by utilizing Cattaneo-Christov heat flux model and chemical processes over an exponentially stretching surface," *Results in Physics*, vol. 8, pp. 397–403, 2018.

[25] S. Noreen, "Magneto-thermo hydrodynamic peristaltic flow of Eyring-Powell nanofluid in asymmetric channel," *Nonlinear Engineering*, vol. 7, no. 2, pp. 83–90, 2018.

[26] W. Ibrahim and B. Hindebu, "Magnetohydrodynamic (MHD) boundary layer flow of eyring-powell nanofluid past stretching cylinder with cattaneo-christov heat flux model," *Nonlinear Engineering*, 2018.

[27] K. Anantha Kumar, B. Ramadevi, and V. Sugunamma, "Impact of lorentz force on unsteady bio convective flow of carreau fluid across a variable thickness sheet with non-fourier heat flux model," *Defect and Diffusion Forum*, vol. 387, pp. 474–497, 2018.

[28] B. Ramadevi, V. Sugunamma, K. Anantha Kumar, and J. V. Ramana Reddy, "MHD flow of Carreau fluid over a variable thickness melting surface subject to Cattaneo-Christov heat flux," *Multidiscipline Modeling in Materials and Structures*, 2018.

[29] K. Anantha Kumar, J. V. Ramana Reddy, V. Sugunamma, and N. Sandeep, "MHD carreau fluid flow past a melting surface with cattaneo-christov heat flux," in *Applied Mathematics and Scientific Computing, Trends in Mathematics*, 336, p. 325, 2019.

[30] R. E. Powell and H. Eyring, "Mechanisms for the relaxation theory of viscosity," *Nature*, vol. 154, no. 3909, pp. 427-428, 1944.

[31] M. Y. Malik, I. Khan, A. Hussain, and T. Salahuddin, "Mixed convection flow of MHD Eyring-Powell nanofluid over a stretching sheet," *A numerical study AIP Advances*, vol. 5, no. 11, Article ID 117118, 2015.

[32] J. N. Reddy, *An Introduction to the Finite Element Method*, McGraw– Hill, New York, NY, USA, 1985.

[33] E. B. G. F. Becker and J. T. Oden, *Finite Elements an Introduction*, Texas Institute for Computational Mechanics, UT Austin, 1981.

[34] O. C. Zienkiewicz and R. L. Taylor, *The Finite Element Method, Volume 1: Basic Formulations and Linear Problems*, McGraw Hill, London, UK, 4th edition, 2013.

[35] W. A. Khan and I. Pop, "Boundary-layer flow of a nanofluid past a stretching sheet," *International Journal of Heat and Mass Transfer*, vol. 53, no. 11-12, pp. 2477–2483, 2010.

[36] M. Goyal and R. Bhargava, "Finite element solution of double-diffusive boundary layer flow of viscoelastic nanofluids over a stretching sheet," *Computational Mathematics and Mathematical Physics*, vol. 54, no. 5, pp. 848–863, 2014.